ACS APPLIED BIO MATERIALS



Article

# A Highly Selective Turn-On Biosensor for Measuring Spermine/Spermidine in Human Urine and Blood

Ratish R. Nair, Snehasish Debnath, Shruti Das, Padmaja Wakchaure, Bishwajit Ganguly, and Pabitra B. Chatterjee

*ACS Appl. Bio Mater.*, **Just Accepted Manuscript** • Publication Date (Web): 22 May 2019



## Just Accepted



is published by the American Chemical Society. 1155 Sixteenth Street N.W., Washington, DC 20036

# A Highly Selective Turn-On Biosensor for Measuring Spermine/Spermidine in Human Urine and Blood

**Ratish R. Nair,[†,‡] Snehasish Debnath,[†,‡] Shruti Das,[†] Padmaja Wakchaure,[†,‡] Bishwajit Ganguly,[*,†,‡] and Pabitra B. Chatterjee[*,†,‡]**

[†]Analytical & Environmental Science Division and Centralized Instrument Facility, CSIR-CSMCRI, G. B. Marg, Bhavnagar, India.

[‡]Academy of Scientific and Innovative Research (AcSIR), CSIR-CSMCRI, G. B. Marg, Bhavnagar, India.

**Corresponding author: pbchatterjee@csmcri.res.in**

**Abstract:** Spermine and spermidine serve as the key biomarkers for early stage cancer diagnosis. This work reports a rapid, highly selective, and non-invasive sensing platform for spermine/spermidine. The hybrid material, developed in this work, has been characterize by UV-vis, IR, powder XRD, SEM, EDX, and rheological studies. Storage modulus (G') and loss modulus (G") measurements infer that embedding boronic acid integrated coumarin soften the agarose gel fibres at room temperature. Stress resistance measurement and subsequent imaging further confirms the softness of the hybrid hydrogel over pure agarose gel and homogeneous distribution of the dye in the hybrid matrix as well. The soft hydrogel with limit-of-detection (LOD) 6 μM showed nearly 27-folds fluorescence enhancement for spermine. The hybrid hydrogel matrix can be useful within a wide concentration window (6 μM-to-2.5 mM spermine). Response time (≤ 7 s) confirms rapid detection ability of the material. Non-interference from various metal ions, common anions, monosaccharides, nucleobases, and amino acids particularly, histidine, arginine, lysine, ornithine, glutamine, etc., makes the hybrid hydrogel suitable for the real-time measurement of spermine in human urinary and blood samples. Furthermore, non-interference from other biogenic amines supports highly selective nature of the hybrid gel. Ability to measure spermine in urinary samples by the probe offers non-invasive nature of the sensing platform. Overall, we envisioned that the hybrid material formulation would be useful for early-stage tumor diagnosis and assessing the recovery of patients undergoing chemotherapeutic treatment.

**Keywords**

Agarose hydrogel, biosensing spermine/spermidine, boronic acid, coumarin, human blood and urine.

## Introduction

Among different biogenic polyamines that are naturally abundant in cells and body fluids of eukaryotes, spermine (a tetracationic biogenic amine, Figure 1) and spermidine (a tricationic bioamine, Figure 1) play crucial role in cell growth and proliferation, immune response, neuron regulation, etc.[1-6] Alteration of spermine/spermidine levels in urine/cells, works as reliable biomarker in many biological deformities like psoriasis, peptic ulcers, and chronic gastritis.[7] These two bioamines also serve as useful indicators for abnormal biochemical processes associated with different types of malignant tumors.[8-12] Accordingly, spermine is considered as the basic tool for early stage detection of any cancer in human body. Monitoring spermine levels in urine and saliva, has also developed a brilliant technique for early phase diagnosis and evaluating the recovery of patients undergoing chemotherapeutic treatment.[13,14] Hence, it becomes imperative to develop diagnostic assays or kits that can detect spermine and spermidine in biofluids with high selectivity and sensitivity in a very small volume of sample.

Ever since Timothy Swager[15] has illustrated the limitations in the use of chromatography, capillary electrophoresis, and immunoassay techniques in the measurement of spermine/spermidine in our body fluids, reports start appearing in the literature on the design and development of optical probes for selective detection of spermine/spermidine. The subject, however, got increased momentum after the seminal report from Hamachi and co-workers[14] in which the authors have described the use of a hybrid hydrogel as an excellent fluorosensor for spermine/spermidine in artificial urine. In this work, we have compiled the literature on this topic in Table 1,[14-34] which divulges that during the past few years, a number of nanoparticles based probes have emerged as the effective probes for the detection purpose. The stimulating contribution from Kim et al. deserves special reference in this context.[23] Later, a few self-assembled systems encompassing different polymer/dye/surfactant/macrocycles/quantum dots have also appeared in the literature for sensing spermine/spermidine in different real-world

samples.[17,18,20,25-27,29] Unfortunately, most of the reported systems suffer from various limitations such as tedious and complex synthetic and purification steps;[16,19,21,23,24,28,30-32] inferior turn-off phenomenon;[18,20,22,25,27,28] interference from other polyamines (e.g. putrescine, histamine, cadaverine, adamantanamine, etc.)/glutathione/NaCl;[14,15,18,21,25,27,28,30,31,33] use of expensive gold nanoparticles;[16,19,23,28,30,31,32] requirement of certain stringent conditions for stability;[18,19,21,23,24,26,28,30-32] inability to function at physiological pH condition;[15,16,30-32] and use of organic solvent in the detection process.[15,24,27,29,34]

We have prepared and investigated a new hybrid material formulation in which mechanosynthesized novel dye 3-((7-hydroxy-4-methylcoumarin)methylene)aminophenylboronic acid (we abbreviated as CB, Figure 1) is incorporated into the matrix of a natural polysaccharide agarose, the latter is a natural polymer that has been extensively used in molecular biology. Powder XRD, SEM-EDX imaging, UV-vis, and rheological techniques subsequently characterized the soft hydrogel matrix, hereafter abbreviated as CB@AG. The hydrogel based sensing platform (Figure 1) showed highly selective and rapid fluorescence enhancement in presence of spermine and spermidine in pure water at physiological pH with 6 μM limit of detection (LOD). Excellent sensory properties of the hydrogel makes it suitable for naked eye detection of spermine in artificial and natural human urinary samples and human blood plasma as well. To the best of our knowledge, this is the first report to explore the potential hydrogel of a boronic acid coupled coumarin dye incorporated agarose polymer formulation that has been intended for non-invasive biosensing of spermine and spermidine in human biofluids.

## Results and Discussion

**Synthesis and Characterization.** Boronic acid integrated coumarin dye CB was prepared by mechanochemical grinding of 3-aminophenylboronic acid and 8-formyl-4-methylumbeliferrone using few drops of methanol in a mortar-pestle. To confirm the formation of CB, powder XRD, IR, NMR ($^{1}$H & $^{13}$C) data of the mechanosynthesized product were compared with the analogous data of CB prepared via traditional solution-based refluxing technique (Figure S1 and Experimental Section). Morphology of the mechanosynthesized CB, obtained from SEM, also displays complete resemblance with the counterpart prepared via conventional refluxing technique (Figure S1). Elemental analysis, NMR ($^{1}$H and $^{13}$C, Figure S2, S3), and ESI-MS (Figure S4) confirms the molecular structure of the dye (shown in Figure 1). Mechanosynthesized CB next mixed with agarose powder in water. After heating the mixture up to 90 $^{\circ}$C, the hydrogel (1 wt %) CB@AG was formed upon cooling the solution to room temperature. Further works have subsequently been carried out to characterize the resulting composite material CB@AG by different analytical techniques.

Comparison of the UV-vis spectrum of CB@AG with that of AG showed a new peak at 354 nm in the former (Figure S5). This provides information about the incorporation of the dye CB into the hydrogel AG. IR spectra of dried AG and CB@AG contain all the pertinent bands due to agarose polymer appearing at 3360, 2920, 1640, 1185, 1080, 930, and 890 cm$^{-1}$ as prominent features (Figure S6). Besides, CB@AG shows a strong band at 1670 cm$^{-1}$ due to the carbonyl CO stretching present in the lactam ring of CB. The structural integrity of the dye CB in the hybrid material was next investigated via powder XRD studies. Comparative PXRD profiles of free CB and CB-embedded hydrogel suggests dye induced crystallinity in the hydrogel CB@AG (Figure 2a), at least in the dry state. PXRD patterns of free CB and CB-embedded hydrogel showed reflections at 2$\theta$= 9.25, 13.25, 15.40, 24.72, 27.85, and 30.50$^{\circ}$ for both the samples. Therefore, confirming successful incorporation of the dye into the hybrid material.

The broad hump at 19° in the hydrogel appears due to the AG matrix and hence, demonstrating the retention of the structural identity and robustness of the dye in the composite.

More compact and dense packing of AG over CB@AG fibres and/or fibre bundles is revealing from FE-SEM images (Figure 2b,c) of the hydrogels. SEM-EDX based elemental mapping confirms dense and homogeneous distribution of boron and nitrogen atoms (Figure 3a,b) in the hydrogel CB@AG. Loading of CB into the hydrogel is complemented further by the EDX spectroscopic analysis and elemental mapping (Figure 3c) that reveals a degree of substitution with boron contents of 14.13 % (by atom). Various rheological properties such as strength, swelling, etc., were performed to explore the properties of the hydrogel. The gelation of 1 % agarose takes place between 40-25 °C and this is well supported in the literature.[35] Accordingly, no further experiment was performed to explore gel formation process. In order to know the strength of the hydrogels, storage modulus (G') and loss modulus (G") values were measured at room temperature. Typically, G' expresses the amount of stored mechanical energy in a viscoelastic material after the application of elastic force of deformation while, G" denotes the viscous response of the material and measures liberated heat energy.[36] Average G' value is greater than the average G" value at 1 Hz frequency indicates elastic behavior of the hydrogel CB@AG (Figure 4).[37] Time dependent variations in G' and G" at 25 °C and 1 Hz constant frequency was monitored using an oscillatory time sweep experiment. Plot shown in Scheme 1 reveals that the initial value of G' was higher than G" value, but gradually decreased with time. Therefore, an intersection has been noticed at a short time interval after the application of pressure. This point indicates liquefaction of the gel.[37]

**Schematic illustration from different characterization data.** Following the elegant demonstration in the literature by Yang et al.[38,39] a schematic model is proposed in Scheme 1, which is based on the results from various analytical studies. Upon heating the agarose solution mixture to 90 °C, a clear yellow agarose solution is formed (as shown in Scheme 1). In this

state, the chains of the biopolymer remain disordered (shown in Scheme 1). Upon gradual cooling of the agarose solution to room temperature, yellow colored homogeneous hydrogel CB@AG (1 wt %) is formed. During this process, the randomly oriented polysaccharide coils reorganized to an ordered state in which weak intermolecular hydrogen bonding interactions (i.e. non-covalent forces) resulted in the formation of double helical arrangements of the biopolymer in the initial stage and latter to a bundles of double helices as shown in Scheme 1.[40] Presence of large number of hydroxyl groups in the helices resulted a 3D network structure of the gel by virtue of further aggregation and cross linking of the strands forming supercoiled assembly (as depicted in Scheme 1).[40,41] UV-vis analysis showed a high-energy absorption band (Scheme 1) that can be assigned to the CB-centered $\pi$-$\pi$* transition in CB@AG.[42] Evidence in support of incorporation of CB into the bundles of AG has been obtained when the IR profile of CB@AG was compared with that of AG. Appearance of a strong band around 1670 $cm^{-1}$ clearly due to the lactam CO functionality. Thus, illustrating the successful integration of the dye CB into the hydrogel matrix. Stretching frequency shift from 1730 $cm^{-1}$ (see Experimental Section and Figure S1) to a lower value (1670 $cm^{-1}$, Figure S6) is presumably due to the H-bonding of CO with the hydroxyl groups of AG. The retention of the gel structure of AG in CB@AG is also apparent from the band positions at 3360 $cm^{-1}$ (axial OH deformation), 2920 $cm^{-1}$ (axial CH deformation), 1640 $cm^{-1}$ (OH bending), and 930 $cm^{-1}$ (3,6-anhidrogalactose).[43] Unfortunately, C=N stretching band at 1630 $cm^{-1}$ overlapped with the absorption band due to the OH bending mode of agarose polymer. Insight information about the packing of CB molecule in CB@AG is apparent from the wide-angle PXRD data of the dried and swollen hydrogels as well. The peaks in the wide-angle region ($2\theta$= 24.72 and 27.85$^{\circ}$) are corresponding to 3.61 and 3.20 Å d-spacing values, respectively. These could be the due to the typical $\pi$-$\pi$ interaction between the aromatic rings.[44,45] The d-spacing of 2.88 Å corresponding to the weak peak at $2\theta$= 30.50$^{\circ}$ indicates intermolecular H-bonding between

boronic OH groups. As described earlier by Ajayaghosh et al., diffraction peak corresponding to the d-spacing 5.74 Å (at 2θ= 15.40˚) can be assigned to the end-to-end distance between two adjacent CB molecules.[44] Equal intense peak at 2θ= 13.25˚ resembles to the d-spacing of 6.68 Å, which could be the width of CB.[45] Interestingly, the crystallinity of CB is lost in swollen hydrogel CB@AG as evidenced from Scheme 1.

SEM analysis was also explored to get information about the morphology of AG and CB@AG hydrogels. Both AG and CB@AG have abundant pores (Figure 3a). SEM images reveal long cylindrical rod-like shapes presumably originated due to the intermolecular H-bonding among polysaccharides.[46] Furthermore, cross-linking of these rods has resulted in the appearance of channels as shown in Figure 2c and Scheme 1. Clearly, the interior of the channel is large enough, even in the dry state, to accommodate the dye (CB) molecules. Obviously, a good number of H-bonding from the boronic acid, phenolate O, and carbonyl CO moieties with the large number of hydroxyl groups of agarose facilitates the loading of CB inside the hydrogel. Elemental mapping using SEM-EDX technique confirms the incorporation and homogenous distribution of B and N in CB@AG (Figure 3 and Scheme 1). Therefore, ascertain the successful incorporation of the dye CB into the hydrogel CB@AG. Analysis of rheological data (shown in Figure 4) reveals higher value of the storage modulus (G') i.e. mechanical energy with regard to loss modulus (G"). Thus, indicating viscoelastic nature of both AG and CB@AG.[37] However, the window displaying linearity is narrow. The average G' and G" values of CB@AG, measured at 25 ˚C, were found to be $9.1 \times 10^3$ and $1.2 \times 10^3$ Pa, respectively. Mechanical strength of CB@AG matrix is revealing undoubtedly from the plot shown in Scheme 1 in which G' and G" is plotted simultaneously against strain and time. Clearly, the time requires for G" to supersedes G' has changed from 11 to 8.93 min upon incorporating CB into the hydrogel. Thus, embedding CB has soften the agar gel fibres. The softness of CB@AG further supported from Scheme 1 that showed that hydrogel CB@AG could only resist 10 %

stress in comparison to 26 % in AG-only hydrogel.[37] The degree of water swelling is lower for CB@AG (5206 % w/w) with respect to AG hydrogel (5870 % w/w). Apparently, hydrophobicity of CB is responsible for this observation. We next investigated the effect of incorporation of the fluorogenic dye CB into natural biopolymer AG as a smart platform in the area of biosensor development.

**Sensing properties of the hydrogel CB@AG.** As already mentioned in the preceding section, the absorption spectrum of CB@AG (Figure S5) showed an absorption peak at 354 nm corresponding to the $\pi \rightarrow \pi^*$ transition in the dye CB and the material is colorless under visible light. CB@AG itself is non-fluorescent and the emission spectrum of the hybrid matrix was measured in the range 380-550 nm following excitation at 370 nm. In literature, sensing ability of boronic acid derivatives toward different carbohydrates has been very well explored.[47-49] Therefore, we started our investigation in the exploration of the excited state sensing properties of CB@AG in presence of different carbohydrates and nucleobases. Emission measurement of CB@AG, without and with the addition of various carbohydrates and nucleobases showed no change in the fluorescence behavior of the hydrogel (Figure 5a). In other two sets of experiments, binding specificities of CB@AG toward different metal ions and common anions in aqueous HEPES buffer were performed. Results shown in Figure 5b and 5c demonstrate insignificant changes in the emission of CB@AG upon addition of the aforementioned two series of analytes. Recently, Tian and co-workers have established an excellent assay for colorimetric visualization of dopamine (an important biogenic amine that functions as crucial neurotransmitter), using boronic acid derived ligand functionalized gold nanoparticles.[50]

To our surprise, sensing properties of CB@AG when studied in presence of different biogenic amines, remarkable fluorescence enhancement (27-folds) of the hybrid hydrogel was observed with spermine at physiological pH condition (Figure 5d). Sky-blue coloration of

CB@AG was noticed under UV lamp (Figure 6a). Moderate emission enhancement (10-folds) was also observed in presence of spermidine. Prior to our observation, only one report has appeared in the literature describing the use of hydrogel in the detection of spermine/spermidine.[14] However, montmorillonite-coumarin based hydrogel of Hamachi et al.[14] showed fluorescence turn-off response. Table 1 listed fourteen different reports on fluorescence based detection for spermine/spermidine. Except gold nanoparticles[16,21] and quantum dots[26] derived probes, most of the other system[14,18,20,22,25,27,28] showed emission turn-off properties. Insensitive behavior of CB@AG towards methionine, arginine, lysine, histidine, and ornithine (Figure 5d) deserves special mention in this context.

The pH variable selective detection of spermine and spermidine by CB@AG was explored in the pH window 2.6-10.6. Results displayed in Figure 6a dictate that CB@AG can work well in the pH range 7.4-10.6. Thus, in this study, all bio-sensing works were performed in HEPES buffer at 7.4 pH. Herein, it is worthwhile to cite few systems that are useful at acidic pHs such as pH 6,[16] 5.5,[15] or even 3.29.[30,32] Control experiments with AG (pure agarose hydrogel) was also performed and the results shown in Figure S7 reveals no affinity of AG for spermine/spermidine.

Response time of the hydrogel was ascertained from the time-scan emission spectral change measurement of CB@AG in presence of spermine/spermidine. Results from Figure 6b indicates short (≤ 7 s) reaction time, which is effective for practical use. It is clearly evident from Table 1 that the detection of spermine/spermidine often challenged by other biogenic amines,[14,18,25,26,31] polyamines,[15,18,21,33] or BSA[28]/histamine[30], etc. Furthermore, biogenic amines such as putrescine and cadaverine prevail in urine. Hence, it becomes imperative to check their interference too while developing sensors to be useful for urinary spermine/spermidine. Selective detection of spermine by CB@AG remain unchanged in occurrence of other biogenic amines (Figure 6c) illustrating the use of CB@AG as an extremely

specific material for spermine. With increasing concentrations of spermine (0-2.5 mM), the emission peak intensity of the matrix gradually improving (Figure 7a). Therefore, CB@AG can measure spermine concentrations in a wide range. In order to estimate the limit of detection (LOD), we plotted $[(F-F_0)/(F_\alpha-F_0)]$ against Log[spermine] as described in our recent article.[51] Here $F_0$, F, and $F_\alpha$ are the fluorescence intensities of the hydrogels without spermine, with spermine at a certain concentration, and in presence of highest concentration of spermine used in the titration experiments, respectively. [spermine] denotes the concentration of spermine. From the plot, calculated LOD was found to be 6 μM (Figure 7b). For instrument free detection of spermine by the hydrogel, naked eye observable LOD was appeared to be 40 μM (Figure 7c). Needless to mention that nanoparticles derived probes offer great LOD, in the order of nanomolar (nM),[16,21,24,26,28,29,30-32] However, their saturation limits also hit at a low spermine concentration (up to several μM). Therefore, these systems are not very useful at a higher spermine concentration.

**Proposed mechanism for selective detection of spermine by CB@AG.** We investigated further the interaction between the dye CB and spermine to provide a tentative working mechanism for the specific binding of spermine with the hybrid hydrogel CB@AG. Using the change in emission peak intensity at 440 nm, Job's plot (Figure S8) was generated from the experimental data that indicates 1:1 binding stoichiometry between CB and analyte. The binding affinity of spermine for CB was determined by performing fluorimetric titration in which increasing addition of tetracationic spermine to the solution of CB in aqueous HEPES buffer solution resulted in the gradual enhancement of the emission peak intensity. Fitting the titration data points using the following non-linear equation 1[51] in which $F_0$ & F denote fluorescence intensities of CB at 440 nm without and with spermine/spermidine, respectively. In equation 1, $F_{max}$ is the fluorescence intensity of CB at 440 nm in the presence of excess amount of spermine/spermidine. The calculated association constant was found to be $5.44 \times 10^3$

$M^{-1}$ (Figure 8a) with spermine. Similar, spectrophotometric titration with the tricationic spermidine provided binding constant $2.02x10^3$ $M^{-1}$ (Figure 8b). Therefore, CB exerts stronger association tendency towards spermine which presumably indicating higher electrostatic interactions and strong intermolecular hydrogen bonding between CB and tetracationic spermine. ESI-mass spectral analysis of the CB-spermine adduct at neutral pH displays a prominent positive ion base peak at *m/z*=176.01, corresponding to the tricationic species $[CB\text{-}H^{+}+spermineH_4]^{3+}$ in the positive ion mode with high relative abundance (Figure S9). Surprisingly, limited information on the association constant values in the area of spermine/spermidine detection has been documented in the literature (not included in Table 1). Binding constants in the range $3.4x10^4$-$2.6x10^7$ $M^{-1}$ were reported for a few self-assembled systems.[18,22,25,27,29] Presumably, self-assembly nature of the probes have resulted moderate-to-high binding constants in these materials.

We have performed the conformational search with MMFF force field and the lowest energy conformers were taken for CB, spermine, and spermidine to calculate the complexation stability for the biogenic amines.[52,53] The single point calculations have been performed using B3lyp/6-31g(d) level of theory to examine the complexation energies of CB with spermine and spermidine.[53] Intermolecularly H-bonded CB-spermine complex was found to be 42.0 kcal/mol more stable than the other H-bonded species i.e. CB-spermidine complex. The proposed binding modes for binding of spermine/spermidine with CB is shown in Figure 9. Therefore, on addition of spermine to CB@AG, intermolecular hydrogen bond formation by the ammonium hydrogens of spermine with the imine nitrogen and boronic OH moieties of CB has resulted enhanced fluorescence emission. Possible hydrogen bonding between spermine and agarose moiety is also occurring.

$$\mathbf{F = F_0 + \frac{F_{max} - F_0}{2}\left\{\left(1 + \frac{[M]}{C_L} + \frac{1}{C_L K}\right) - \sqrt{\left(1 + \frac{[M]}{C_L} + \frac{1}{C_L K}\right)^2 - 4 * \frac{[M]}{C_L}}\right\}} \quad \text{---------- (1)}$$

To know more about the properties of CB@AG in the excited state, we also studied excited state decay behavior of the dye CB by time correlated single photon counting (TCSPC) at $\lambda_{exi}$=375 nm and $\lambda_{emi}$=440 nm (due to our limitation, we could not perform similar studies with the hybrid hydrogel). Single exponential fitting of the data points were performed to provide best decay fit. The quantum yield ($\Phi_f$) of CB was estimated to be 0.012 and it increased to ca. 18-folds in presence of spermine ($\Phi_f$= 0.218). The fluorescence lifetime ($\tau$) of CB (5.51 ns) in aqueous HEPES buffer has decreased to 5.35 ns when spermine was added the probe's solution (Figure 10). This indicates that CB-spermine adduct deactivates at a faster rate than CB alone in the excited state. Following the equations $k_r + k_{nr} = \tau^{-1}$ and $k_r = \Phi_f/\tau$, we calculated radiative ($k_r$) and total non-radiative rate ($k_{nr}$) constants which are compiled in Table 2. Data shown in Table 2 clearly indicates that both $k_r$ and $k_{nr}$ are the responsible factors for the fluorescence enhancement of CB@AG with spermine. Low quantum yield and high $k_{nr}$ value indicates involvement of the non-bonding electrons of the imine nitrogen atom in the photo excited electron transfer (PET) process.[54] As a result, radiative decay of the dye CB was hindered causing turn-off property in the probe CB. However, when spermine was added to this quenched system, hydrogen bonding from the imine nitrogen of CB to the ammonium moiety of spermine (Figure 9) significantly reduces the deactivating pathway i.e. PET process.[54] The diminishing or restriction in the PET process due to the formation of intermolecular H-bonding has resulted in the increase of $\Phi_f$ and $k_r$ values in the CB-spermine complex. Consequently, turn-on response of the hydrogel CB@AG was observed upon addition of spermine.

**Analysis of spermine in bio-fluids urine and plasma.** We have examined the applicability of the new hydrogel sensor CB@AG for practical samples such as human urine (both artificial

and natural) and blood plasma. Collection of urine is non-invasive and easy. Therefore, considered as a convenient approach for investigating prostate cancer biomarkers. Hence, the potential of the material CB@AG was first investigated by performing spermine analysis in artificial urine, the latter was prepared following the procedure of Hamachi et al.[14] Aliquot of urine sample was spiked with known amount of spermine and emission spectrum of the urine sample was acquired. Fluorescence of the urine samples increased linearly. The concentration of spermine was extracted from the calibration curve shown in Figure 11. The estimated amounts of spermine in each aliquot is quite satisfactorily agreeing with the calculated values. We next have performed a separate analysis to assess whether the hybrid material will be useful for the estimation of spermine level in a practical situation. In this context, it is worthwhile to mention that in the literature[14,15] it has been well documented that the elevated levels of spermine (~10 μM)/spermidine (~40-50 μM) in human urine can be considered as a promising biochemical marker for many types of rapidly growing tumors. Hence, spiked human urinary sample was also tested fluorimetrically using the hybrid gel CB@AG. Emission peak intensity at 440 nm was used to determine the concentration of spermine in healthy human urine donated by an individual. Results shown in Figure 11 suggests that the title hydrogel CB@AG is capable for sensitive detection of spermine in human urine. Final demonstration of the potential utility of the hydrogel for real time monitoring of spermine, CB@AG was also further studied as a bio-sensory material to detect and estimate spermine in human blood plasma with standard addition method as above. In Figure 11, gradual increase of emission intensity at 440 nm is noticed with rise of spermine concentration in human plasma. The specific detection of spermine in human plasma spiked with other biogenic amines was also confirmed experimentally. The overall detection ability of the hydrogel matrix to measure spermine in urine and plasma samples falls 2-4 % short than the sensitivity in aqueous solution. In sum, the

hybrid hydrogel CB@AG can detect spermine/spermidine efficiently in relatively complex bio-fluids such as human urine and plasma for carrying out early preventive procedures.

Reliability of the present assay has been validated by measuring the spermine concentrations by the conventional HPLC method. Briefly, 200, 100, 50, 25, 12.5, and 6.25 μM spermine solution in water was mixed with 100 μM hexamethylenediamine (taken as internal standard, IS). Following the treatment steps, described in the Experimental Section,[55] two different calibrations plots (using two different types of detectors in the HPLC i.e. UV versus fluorescence based detectors) were generated by plotting ratio of the peak area of spermine to IS versus amount of injected spermine (Figure 12). Linear relationship within 3-100 μM regime is clearly evident from Figure 12. Representative chromatogram of standard spermine solution in presence of hexamethylenediamine is shown in Figure S10. The procedure was repeated thrice and the error bar in Figure 12 denotes standard deviation. Next, an unknown dilution was prepared from 100 μM spermine stock solution and its concentration was measured by fluorescence technique using the title probe CB@AG and traditional HPLC method as well (Figure 12). Experimentally observed values (shown in Figure 12), by both the methods, validate (at more than 94 % confidence level) the assay presented in this article.

## Conclusions

Herein, we developed a novel hybrid hydrogel CB@AG by incorporating boronic acid bearing coumarin dye into agarose matrix. This hybrid material can selectively and rapidly detect two important biomarkers spermine and sermidine via fluorescence turn-on fashion that is observable by the naked eyes. Successful integration of coumarin dye was validated by different analytical techniques that included UV-vis, IR, PXRD, SEM, and rheology. EDX spectroscopic analysis and elemental mapping provided information in favor of successful and homogeneous loading of CB into the hydrogel matrix. Notably, immobilizing the dye CB has

soften the agar gel fibre. Both stress resistance and degree of water swelling are lowered in the hybrid hydrogel compared to that of the bare gel AG. The emission intensity of the material enhances significantly with biogenic amines spermine (27-folds) and spermidine (10-folds). While, introduction of other series of analytes such as carbohydrates, nucleobases, metal ions, and common anions resulted no change in the emission intensity of CB@AG. Fluorescence enhancement of CB@AG with spermine/sermidine is attributed to the hydrogen bonding from the imine nitrogen of CB that significantly decreases the PET process that has been happening in free CB. The single point calculations using B3lyp/6-31g(d) level of theory reveals that the CB-spermine complex is 42.0 kcal/mol more stable than CB-spermidine complex CB@AG represents the first example of a hybrid hydrogel in which a mechanochemically synthesized dye has been incorporated into the matrix of a natural polysaccharide that can detect the biogenic polyamines spermine/spermidine in pure aqueous buffer. More interestingly, presented smart platform can be used to measure spermine levels in human urine and blood plasma. Excitingly, present results also established that use of this type of hybrid soft materials have strong potential for designing biosensors for a range of analytes that are crucial for point-of-care clinical purposes and further research on this topic is currently underway.

## Experimental Section

**Materials.** 3-aminophenylboronic acid, 4-methyl-7-hydroxycoumarin, paraformaldyhe, tetrabutylammonium and sodium salts of different anions, perchlorate salts of different metals ions, carbohydrates, nucleobases, sugars, amino acids, biogenic amine, HEPES, agarose, anthracene, dansyl chloride, hexamethylenediamine, and other analytical reagents were purchased from Aldrich and used directly. All other chemicals and solvents were reagent grade and acquired from local suppliers. Signalling precursor 8-formyl-7-hydroxy-4-methyl coumarin (FHMC) was obtained following reported procedure.[56] Human blood plasma was collected from Bhavnagar blood bank and stored at -20 ˚C. A healthy individual donated urine

sample, which was stored at -20 ˚C. Quantum yield was measured using anthracene and the procedure available in the literature[57,58] was followed.

**Instrumentations.** Field Emission Scanning Electron Microscope (FE-SEM) was performed in a JEOL-JSM 7100F with an accelerating voltage of 15 kV. Images were taken at magnification values of 100x, 250x, 7000x, and 10000x and processed for boron and nitrogen distribution using EDX spectroscopy. An accelerating voltage of 15 kV at 50 μm magnification was also used to collect the EDX spectrum. All data were processed using Oxford INCA software. LEICA EM ACE 200 plasma-sputtering device was used. Elemental analysis was carried out in a model 2400 Perkin-Elmer elemental analyser. Emission and absorption spectra were collected on Fluorolog FL 1065 Horiba Jobin Yvon Spectrometer and Shimadzu 3600 UV-Vis-NIR spectrophotometer, respectively. Powder X-ray diffraction patterns were recorded with a PAN Analytical EMPYREAN instrument (Made in Netherland) operated at 40 kV and 30 mA and standard silicon sample was used for calibration. Ni-filtered $CuK_{\alpha}$ ($\lambda$= 0.15406 nm) radiation was used. IR spectra were recorded using Perkin Elmer Spectrum GX FT-IR System. Melting points of the dye CB was measured using Mettler-Toledo FP-62 instrument. Proton and $^{13}C$ NMR experiments were carried out on a JEOL Resonance ECZR 600 MHz FT-NMR instrument. Fluorescence lifetime measurements were performed by the method of time correlated single-photon counting using Edinburgh instrument OB 920 spectrofluorometer with nanosecond diode laser at 375 nm as the light source. For all lifetime measurements, a single exponential iterative fitting program analyzed the fluorescence decay curves. Lifetime studies were performed by following the procedure described in our earlier report.[51] Rheological studies were carried out by Physica MCR 301 rheometer (Anton Paar) using a pp50 (diameter 49.973 mm) probe. For freeze drying, Vir Tiz benchtop freeze-dryer was used. Grinding experiments were performed using Agate mortar-pestle. ESI-MS was measured on a Micromass Q-ToF microTM and Agilent technologies 6545 Q-TOF

LCMS/Infinity 2 HPLC. Thermo Scientific Orion Versa-star Advanced Electrochemistry meter was used for pH adjustment. Waters made HPLC system with attached 2996 photodiode array detector, 2695 separation module, and 2414 refractive index detector operated by Breeze 2 software was used. Fluorescence based detector system RF-10AXL with SPD-M20A prominence diode array detector of Shimadzu was also used for recording HPLC.

**Mechanochemical synthesis of the dye 3-((7-hydroxy-4-methylcoumarin)methylene)aminophenylboronic acid (CB).** FHMC (1 mmol) and 3-aminophenylboronic acid (1 mmol) were taken in a mortar and thoroughly ground using a pestle. Few drops of methanol was added to the mixture and uniformly ground for another 10 min. TLC was used to monitor the reaction progress. On completion of the reaction, saffron colored solid was obtained. The precipitates was washed with cold methanol and dried further. Recrystallization of the solid was carried out using acetonitrile. Yield: 80 % (recrystallized). MP: > 235 °C. IR bands ($cm^{-1}$) 3412, 2920, 1730, 1630, 1587, 1485, 1389, 1330, 1228, 1088, 843, 707. $^{1}H$ NMR (DMSO-$d_6$, 600 MHz) δ (ppm) =9.27 (s, 1H), 7.87 (s, 1H), 7.78 (d, 1H, J=9 Hz), 7.74 (d, 1H, J=7.2 Hz), 7.53 (d, 1H, 7.8 Hz), 7.44 (t, 1H, J=7.8 Hz), 6.91 (d, 1H, J=9Hz), 6.22 (s, 1H), 2.39 (s, 3H). $^{13}C$ NMR (DMSO-$d_6$, 150 MHz) δ (ppm) =18.28, 106.03, 110.18, 110.64, 114.38, 123.19, 126.21, 128.74, 130.45, 130.59, 133.43, 144.96, 153.99, 156.12, 159.09. Anal. Calcd. for $C_{17}H_{14}BNO_5$: C, 63.19; H, 4.37; N, 4.34. Found: C, 62.90; H, 4.31; N, 4.26. ESI-MS (-ive, methanol, m/z): 322.49 [$M-H^+$]. UV-vis (0.25 % DMSO in $H_2O$) [$\lambda_{max}$, nm (ε, $Lmol^{-1}cm^{-1}$)]: 278 (8950); 354 (15350).

**Procedure for solution based synthesis of CB.** FHMC (1 mmol) dissolved in 20 mL methanol was added to a solution of 3-aminophenylboronic acid (1 mmol, taken in the 10 mL of the same solvent). The mixture was refluxed for ca. 3-4 h and then allowed to cool at room temperature to get saffron colored precipitates. The precipitates was filtered and washed with

cold methanol and recrystallized from acetonitrile. Yield: 81 % (recrystallized). MP: > 235 °C. IR bands ($cm^{-1}$) 3415, 2923, 1732, 1628, 1584, 1483, 1387, 1332, 1225, 1086, 841, 708. $^{1}H$ NMR (DMSO-d6, 600 MHz) δ (ppm) =9.28 (s, 1H), 7.85 (s, 1H), 7.79 (d, 1H, J=9 Hz), 7.75 (d, 1H, J=7.2 Hz), 7.52 (d, 1H, 7.8 Hz), 7.42 (t, 1H, J=7.8 Hz), 6.90 (d, 1H, J=9Hz), 6.20 (s, 1H), 2.37 (s, 3H). $^{13}C$ NMR (DMSO-d6, 150 MHz) δ (ppm) =18.22, 106.13, 110.14, 110.59, 114.34, 123.16, 126.41, 128.64, 130.55, 130.79, 133.33, 144.86, 153.94, 156.20, 159.19. Anal. Calcd. for $C_{17}H_{14}BNO_5$: C, 63.19; H, 4.37; N, 4.34. Found: C, 62.15; H, 4.22; N, 4.19. ESI-MS (-ive, m/z): 322.49 [$M-H^+$]. UV-vis (DMSO-$H_2O$) [$\lambda_{max}$, nm (ε, $Lmol^{-1}cm^{-1}$)]: 276 (8945); 354 (15360).

**Synthesis of the hybrid hydrogel CB@AG.** Solution of CB (2 mg) was diluted to 20 mL using HEPES buffer of pH 7.4. The resulting solution was heated to 90 ˚C under stirring and subsequently 200 mg of agarose was added to the solution. After the formation of transparent solution, the heating was turned off and the solution gradually cooled to room temperature. On cooling, the hybrid hydrogel i.e CB@AG was formed, which was further used for various sensing experiments after proper characterization of the material.

**Measurement of degree of swelling.** Hydrogel CB@AG was kept in water overnight and then weighed. The sample was dried completely by lyophilization. The lyophilized and pre-weighed hydrogel was submerged in water separately and was incubated in a shaker (INFORS AGCH-4103) at a speed of 2 g at 37 °C. Next, the hydrogel was removed at a specific time interval. Excess water was wiped off and weight was recorded. The swelling % (w/w) was determined from the following equation:

$$\text{Swelling (\%)} = \frac{W_{\text{Swollen}} - W_{\text{Dried}}}{W_{\text{Dried}}} \times 100 \quad \text{---------- (2)}$$

where, $W_{Swollen}$ and $W_{Dried}$ are the weights of swollen and dry hydrogels, respectively. These experiments were performed in triplicates and average values are reported.

**Experimental procedure for studying hydrogel morphology and chemical composition.** Hydrogel was freezed overnight at -20 °C and lyophilized further to obtain dried scaffolds. After gold coating using plasma-sputtering coater, thin sections of the dried sample was studied under FE-SEM for morphological analysis. Elemental percentage and distribution in the gel matrix was performed by EDX analysis and elemental mapping of the lyophilized gel.

**Procedure for fluorimetric studies with CB@AG hydrogel.** For carrying out different fluorimetric studies, cubes (100 mg) of CB@AG was taken and dipped into 2.5 mM solutions of different analytes. Fluorescence spectra were recorded after exciting at 370 nm. For fluorescence titration experiments, stocks of spermine was prepared by increasing its concentrations from 0 to 5 mM in aqueous HEPES (20 mM) buffer. 20 μM solution of CB (0.25 % DMSO in aqueous HEPES) was used for titration and different stocks of spermine was prepared by increasing its concentrations from 0-10 mM in aqueous HEPES buffer. From titration data points, binding constant and LOD were determined following the equations already mentioned earlier.

**Artificial urine preparation.** Artificial urine was prepared using the literature reported method of Hamachi and co-workers.[14] In brief, 1.1 mM lactic acid, 2.0 mM citric acid, 25 mM $NaHCO_3$, 170 mM urea, 2.5 mM $CaCl_2$, 90 mM NaCl, 2.0 mM $MgSO_4$, 10 mM $Na_2SO_4$, 7.0 mM $KH_2PO_4$, 7.0 mM $K_2HPO_4$, and 25 mM $NH_4Cl$ was mixed in water. Solution pH was set to 6.0 using 1.0 M HCl. Artificial urine was used for making spermine or spermidine solutions.

**Procedure for detection of spermine in artificial and human urine.** 20 mL human and artificial urine samples were taken in a 50 mL centrifuge tube and the supernatant was collected after removing the precipitates obtained upon centrifugation at 3950 g for 15 min of the mixture. The urine sample, so obtained, was spiked next with different levels of spermine. Each

mL of this spermine solution was treated with a small cube of CB@AG and fluorescence of the hydrogel was measured next.

**Procedure for detection of spermine in human blood plasma.** Human blood was collected from local blood bank and stored at -20 ˚C. Blood sample was spiked with different levels of spermine and then centrifuged for 30 min at 15880 g (maintaining 4 ˚C temperature). The supernatant was collected and for each mL of the supernatant or plasma, 3 mL acetone was added. Proteins precipitated at this stage was further centrifuged at 3950 g for 10 min and the supernatant was collected and diluted with Millipore water. Each mL of spermine solution was treated with a small cube of CB@AG and fluorescence was measured.

**Preparation of standard solution for HPLC experiment.** 20.2 mg spermine was dissolved in 100 mL HCl solution (0.1 mol/L) to make 1 mM stock solution. Next, the stock solution was diluted to 200, 100, 50, 25, 12.5, and 6.25 μM. Similarly, 1 mM stock solution of hexamethylenediamine (11.6 mg in 0.1 mol/L HCl) was prepared and diluted to 100 μM. This solution was used as internal standard (IS) in the HPLC experiments. Saturated solution of sodium carbonate was also prepared in 100 mL water.

**Formation of dansyl derivatives.** Dansylated derivatives were prepared by modifying the method of Kabra *et al*.[55] 2 mL of different spermine solutions (6.25 to 200 μM in 0.1 mol/L HCl) were taken in a set of centrifuge tubes and then 2 mL of hexamethylenediamine (100 μM) was added to each of the tubes. 2 mL saturated aqueous sodium carbonate solution along with 2 mL of dansyl chloride (37 mM in acetone) was next added to each tubes. The aliquots were properly capped and vortexed. The solutions were then subjected to 70 °C in a water bath for 30 min. Afterwards, dansylated products were extracted with 6 mL ethyl acetate. 1 mL from the upper phase was harvested under high-speed centrifugation (3950 g) and used for HPLC experiments.

**High performance liquid chromatography (HPLC) analysis.** Reversed phase (RP) HPLC was carried out by C18 column (100 Å; mesh size 5 μm) of 150 mm length and 4.6 mm internal diameter. Column temperature was kept at 30 °C. Gradient elution was performed with a mobile phase consisting of methanol (solvent A) and HPLC grade water (solvent B). The applied gradient program was 75 % solvent A for first 10 min, 92 % of solvent A for the following 7 min, and 100 % of solvent A for the last 8 min. Additionally 75 % solvent A was ran for 5 min to reach initial condition and stabilisation of the mobile phase. The flow rate was adjusted to 0.8 mL/min at 30 °C. The volume of sample injected for each set was 20 μL. The UV detector was set at 254 nm. Parameters, conditions, and recipe used for UV detector based HPLC experiment was also used for fluorescence detector based HPLC experiments. The excitation wavelength was 430 nm and emission wavelength was 515 nm as reported in literature.[59]

## Associated Content

**Supporting Information Available:** Figure S1-S10. This material is available free of charge on the ACS Publications website at http://pubs.acs.org.

## Author Information

### Corresponding Author

*(P.B.C.) E-mail: pbchatterjee@csmcri.res.in

*(B.G.) E-mail: ganguly@csmcri.res.in

### Notes

The authors declare no competing financial interest.

### ORCID

Pabitra B. Chatterjee: 0000-0003-2741-3684

Bishwajit Ganguly: 0000-0002-9858-3165

**Acknowledgement**

The authors acknowledge the supports from CSIR, New Delhi under MLP 0207 and 0018. RRN and SD acknowledges CSIR for their SRF and JRF, respectively. We also acknowledge the AESD&CIF of CSMCRI for analytical support. This manuscript bears CSMCRI registration number 168/2018.

## References

(1) Mandal, S.; Mandala, A.; Johansson, H. E.; Orjalob, A. V.; Park, M. H. Depletion of Cellular Polyamines, Spermidine and Spermine, Causes a Total Arrest in Translation and Growth in Mammalian Cells. *Proc. Natl. Acad. Sci. U.S.A.* **2013**, *110*, 2169-2174.

(2) Lefevre, P. L. C.; Palin, M. F.; Murphy, B. D. Polyamines On the Reproductive Landscape. *Endocrine Rev.* **2011**, *32*, 694-712.

(3) Pegg, A. E. The function of spermine. *Intl. Uni. Biochem. Mol. Biol.* **2014**, *66*, 8-18.

(4) Bachrach, U. Polyamines and Cancer: Minireview Article. *Amino Acids* **2004**, *26*, 307-309.

(5) Clarke, R. A.; Schirra, H. J.; Catto, J. W.; Lavin, M. F.; Gardiner, R. A. Markers for Detection of Prostate Cancer. *Cancers*, **2010**, *2*, 1125-1154.

(6) Cohen, S. S. A Guide to Polyamines, *Oxford University Press*, USA, **1998**.

(7) Stewart, T. M.; Sierra, J. C.; Piazuelo, M. B.; Mera, R. M.; Chaturvedi, R.; Bravo, L. E.; Correa, P.; Schneider, B. G.; Wilson, K. T.; Casero, R. A. Epigenetic Silencing of miR-124 Prevents Spermine Oxidase Regulation: Implications For Helicobacter Pylori-Induced Gastric Cancer. *Oncogene* **2016**, *35*, 5480-5488.

(8) Chen, Y.; Huang, Z.; Zhao, H.; Xu, J. F.; Sun, Z.; Zhang, X. Supramolecular Chemotherapy: Cooperative Enhancement of Antitumor Activity by Combining Controlled Release of Oxaliplatin and Consuming of Spermine by Cucurbit[7]uril. *ACS Appl. Mater. Interfaces* **2017**, *9*, 8602-8608.

(9) Schipper, R. G.; Romijn, J. C.; Cuijpers, V. M. J. I.; Verhofstad, A. A. J. Polyamines and Prostatic Cancer. *Biochem. Soc. Trans.* **2003**, *31,* 375-380.

(10) Ishikawa, S.; Sugimoto, M.; Kitabatake, K.; Sugano, A.; Nakamura, M.; Kaneko, M.; Ota, S.; Hiwatari, K.; Enomoto, A.; Soga, T.; Tomita, M.; Iino, M. Identification of Salivary Metabolomic Biomarkers for Oral Cancer Screening. *Sci. Rep.* **2016,** *6,* 1-7.

(11) Lima, A. R.; Bastos, M. L.; Carvalho, M.; Pinho, P. G. Biomarker Discovery in Human Prostate Cancer: an Update in Metabolomics Studies. *Trans. Oncol.* **2016,** *9,* 357-370.

(12) Casero, A.; Marton, L. J. Targeting Polyamine Metabolism and Function in Cancer and other Hyperproliferative Diseases. *Nat. Rev. Drug Discovery* **2007**, *6*, 373-390.

(13) Stewart, T. R. M.; Woster, P. M.; Casero, R. A. Targeting Polyamine Metabolism for Cancer Therapy and Prevention. *Biochem. J*. **2016**, *473*, 2937-2953.

(14) Ikeda, M.; Yoshii, T.; Matsui, T.; Tanida, T.; Komatsu, H.; Hamachi, I. Montmorillonite-Supramolecular Hydrogel Hybrid for Fluorocolorimetric Sensing of Polyamines. *J. Am. Chem. Soc.* **2011**, *133*, 1670-1673.

(15) Satrijo, A.; Swager, T. M. Anthryl-Doped Conjugated Polyelectrolytes as Aggregation-Based Sensors for Nonquenching Multicationic Analytes. *J. Am. Chem. Soc*. **2007**, *129*, 16020-16028.

(16) Rawat. K. A.; Bhamore, J. R.; Singhal, R. K.; Kailasa, S. K. Microwave Assisted Synthesis of Tyrosine Protected Gold Nanoparticles for Dual (Colorimetric and Fluorimetric) Detection of Spermine and Spermidine in Biological Samples. *Biosens. Bioelectron.* **2017**, *88,* 71-77.

(17) Zhong, H.; Liu, C.; Ge, W.; Sun, R.; Huang, F.; Wang, X. Self-Assembled Conjugated Polymer/Chitosan-graft-Oleic Acid Micelles for Fast Visible Detection of Aliphatic Biogenic Amines by "Turn-On" FRET. *ACS Appl. Mater. Interfaces* **2017**, *9*, 22875-22884.

(18) Malik, A. H.; Hussain, S.; Iyer, P. K. Aggregation-Induced FRET via Polymer-Surfactant Complexation: A New Strategy for the Detection of Spermine. *Anal. Chem.* **2016**, *88*, 7358-7364.

(19) Martínez, N. J.; Béjar, M. G.; Martínez, Y. M.; Falcó, P. C.; Prieto, J. P. Sensitive and Selective Plasmonic Assay for Spermine as Biomarker in Human Urine. *Anal. Chem*. **2014**, *86*, 1347-1351.

(20) Tu, J.; Sun, S.; Xu, Y. A Novel Self-Assembled Platform For the Ratiometric Fluorescence Detection of Spermine. *Chem. Commun*. **2016**, *52*, 1040-1043.

(21) Yao, Y.; Zhou, Y.; Dai, J.; Yue, S.; Xue, M. Host–Guest Recognition-Induced Color Change of Water-Soluble Pillar[5]Arene Modified Silver Nanoparticles for Visual Detection of Spermine Analogues *Chem. Commun*. **2014**, *50*, 869-871.

(22) Kostereli, Z; Severin, K. Fluorescence Sensing of Spermine with a Frustrated Amphiphile. *Chem. Commun*. **2012**, *48*, 5841-5843.

(23) Kim, T.; Park, J.; Kim, Y. A Gold Nanoparticle-Based Fluorescence Turn-On Probe for Highly Sensitive Detection of Polyamines. *Chem. Eur. J*. **2011**, *17*, 11978-11982.

(24) Chopra, S.; Singh, A.; Venugopalan, P.; Singh, N.; Kaur, N. Organic Nanoparticles for Visual Detection of Spermidine and Spermine in Vapors and Aqueous Phase. *ACS Sustainable Chem. Eng*. **2017**, *5*, 1287-1296.

(25) Liu, K.; Yao, Y.; Kang, Y.; Liu, Y.; Han, Y.; Wang, Y.; Li, Z.; Zhang, X. A. Supramolecular Approach to Fabricate Highly Emissive Smart Materials. *Sci. Rep.* **2013,** *3,* 2372-2379.

(26) Tawfika, S. M.; Shima, J.; Spezialec, D. B.; Sharipova, M.; Lee, Y. I. Novel "turn off-on" Sensors for Highly Selective and Sensitive Detection of Spermine Based on Heparin-Quenching of Fluorescence CdTe Quantum Dots-coated Amphiphilic Thiophene Copolymers. *Sens. Actuators B* **2018**, *257,* 734-744.

(27) Jianga, G.; Zhua, W.; Chena, Q.; Lia, X.; Zhang, G.; Lia, Y.; Fana, X.; Wang, J. Selective Fluorescent Probes for Spermine and 1-adamantanamine Based on the Supramolecular Structure Formed Between AIE-active Molecule and Cucurbit[n]urils. *Sens. Actuators B* **2018**, *261*, 602-607.

(28) Kuo, P. C.; Lien, C. W.; Mao, J. Y.; Unnikrishnan, B.; Chang, H. T.; Lin, H. J.; Huang, C. C. Detection of Urinary Spermine by Using Silver-gold/Silver chloride Nanozymes. *Anal. Chim. Acta* **2018**, *1009*, 89-97.

(29) Singh, P.; Mittal, L. S.; Bhargava, G.; Kumar, S. Ionic Self-Assembled Platform of Perylenediimide-Sodium Dodecylsulfate for Detection of Spermine in Clinical Samples. *Chem. Asian J.* **2017,** *12,* 890-899.

(30) Tsoi, T. H.; Gu, Y. J.; Lo, W. S.; Wong, W. T.; Wong, W. T.; Ng, C. F.; Lee, C. S.; Wong, K. L. Study of the aggregation of DNA-capped gold nanoparticles: a smart and flexible aptasensor for spermine sensing. *Chem. Plus Chem.* **2017,** *82*, 802-809.

(31) Wang, J.; Wu, Z. L.; Zhang, H. Z.; Li, Y. F.; Huang, C. Z. Selective Colorimetric Analysis of Spermine Based on the Cross-Linking Aggregation of Gold Nanoparticles Chain Assembly. *Talanta* **2017**, *167*, 193-200.

(32) Liu, Z. D.; Zhu, H. Y.; Zhao, H. X.; Huang, C. Z. Highly Selective Colorimetric Detection of Spermine in Biosamples on Basis of the Non-Crosslinking Aggregation of ssDNA-Capped Gold Nanoparticles. *Talanta* **2013**, *106*, 255-260.

(33) Fletcher, J. T.; Bruck, B. S. Spermine Detection via Metal-mediated Ethynylarene 'turn-on' Fluorescence Signaling. *Sens. Actuators B* **2015**, *207*, 843-848.

(34) Tanima, D.; Imamura, Y.; Kawabata, T.; Tsubaki, K. Development of Highly Sensitive and Selective Molecules for Detection of Spermidine and Spermine. *Org. Biomol. Chem.* **2009**, *7*, 4689-4694.

(35) Labropaulos, K. C.; Rangarajan, S.; Niesz, D. E.; Danforth, S. C. Dynamic Rheology of Agar Gel Based Aqueous Binders. *J. Am. Ceram. Soc.* **2001**, *84*, 1217-1224.

(36) Zhou, Y.; Yang, H. Effects of Calcium Ion on Gel Properties and Gelation of Tilapia (*Oreochromis niloticus*) Protein Isolates Processed with pH Shift Method. *Food Chem.* **2019**, *277*, 327-335.

(37) Singh Chandel, A. K.; Nutan, B.; Raval, I. H. Jewrajka, S. K. Self-Assembly of Partially Alkylated Dextran-graft-poly[(2-dimethylamino)ethyl methacrylate] Copolymer Facilitating Hydrophobic/Hydrophilic Drug Delivery and Improving Conetwork Hydrogel Properties. *Biomacromolecules* **2018**, *19*, 1142-1153.

(38) Sow, L. C.; Tan S. J.; Yang, H. Rheological Properties and Structure Modification in Liquid and Gel of Tilapia Skin Gelation by the Addition of Low Acyl Gellan. *Food Hydrocolloids* **2019**, *90*, 9-18.

(39) Sow, L. C.; Chong, J. M. N.; Liao, Q. X.; Yang, H. Effects of k-Carrageenan on the Structure and Rheological Properties of Fish Gelatin. *J. Food. Eng*. **2018**, *239*, 92-103.

(40) Stellwagen, J.; Stellwagen, N. C. Internal Structure of the Agarose Gel Matrix. *J. Phys. Chem.* **1995**, *99*, 4247-4251.

(41) Liu, J.; Yang, X.; Wang, K.; Wang, Q.; Ji, H.; Wu, C.; Li, J.; He, X.; Tang, J.; Huang, J. Combining Physical Embedding and Covalent Bonding for Stable Encapsulation of Quantum Dots into Agarose Hydrogels. *J. Mater. Chem.* **2012**, *22,* 495-501.

(42) Mudhulkar, R.; Nair, R. R.; Raval, I. H.; Haldar, S.; Chatterjee, P. B. Visualizing $Zn^{2+}$ in Living Whole Organism Artemia by a Natural Fluorimetric Intermediate Siderophore. *Chem. Selct.* **2017**, *2,* 6407-6412.

(43) Hu, Z.; Hong, P.; Liao, M.; Kong, S.; Huang, N.; Ou, C.; Li, S. Preparation and Characterization of Chitosan-Agarose Composite Films. *Materials* **2016**, *816*, 1-9.

(44) Kartha, K. K.; Babu, S. S.; Srinivasan, S.; Ajayaghosh, A. Attogram Sensing of Trinitrotoluene with Self-Assembled Molecular Gelator. *J. Am. Chem. Soc*. **2012**, *134*, 4834-4841.

(45) Ma, Y.; Ma, H.; Yang, Z.; Ma, J.; Su, Y.; Li, W.; Lei, Z. Methyl Cinnamate-Derived Fluorescent Rigid Organogels Based on Cooperative p–p Stacking and·C=O···π Interactions Instead of H-Bonding and Alkyl Chains. *Langmuir* **2015**, *31*, 4916-4923.

(46) Ratajska-Gadomska, B.; Gadomski, W. Water Structure in Nanopores of Agarose Gel by Raman Spectroscopy. *J. Chem. Phys.* **2004**, *121*, 12583-12588.

(47) Huang, Y. -J.; Ouyang, W. -J.; Wu, X.; Li, Z.; Fossey. J. S.; James, T. D.; Jiang, Y. -B. Glucose Sensing via Aggregation and the Use of "Knock-Out" Binding To Improve Selectivity. *J. Am. Chem. Soc*. **2013**, *135*, 1700-1703.

(48) Liu, Y.; Deng, C.; Tang, L.; Qin, A.; Hu, R.; Sun, J. Z.; Tang, B. Z. Specific Detection of D-Glucose by a Tetraphenylethene-Based Fluorescent Sensor. *J. Am. Chem. Soc*. **2011**, *133*, 660-663.

(49) DiCesare, N.; Lakowicz, J. R. New Color Chemosensors for Monosaccharides Based on Azo Dyes. *Org. Lett*. **2001**, *3*, 3891-3893.

(50) Kong, B.; Zhu, A.; Luo, Y.; Tian, Y.; Yu, Y.; Shi, G. Sensitive and Selective Colorimetric Visualization of Cerebral Dopamine Based on Double Molecular Recognition. *Angew. Chem. Int. Ed*. **2011**, *50*, 1837-1840.

(51) Nair, R. R.; Raju, M.; Jana, K.; Mondal, D.; Suresh, E.; Ganguly, B.; Chatterjee, P. B. Instant Detection of Hydrogen Cyanide Gas and Cyanide Salts in Solid Matrices and Water by using Cu-II and Ni-II Complexes of Intramolecularly Hydrogen Bonded Zwitterions *Chem. Eur. J.* **2018**, *24*, 10721-10731.

(52) Hehre, W. J. A Guide to Molecular Mechanics and Quantum Chemical Calculations, Spartan'14 Wavefunction, Inc. Irvine, CA. **2003**.

(53) Frisch, M. J.; Trucks, G. W.; Schlegel, H. B.; Scuseria, G. E.; Robb, M. A.; Cheeseman, J. R.; Scalmani, G.; Barone, V.; Mennucci, B.; Petersson, G. A.; Nakatsuji, H.; Caricato, M.; Li, X.; Hratchian, H. P.; Izmaylov, A. F.; Bloino, J.; Zheng, G.; Sonnenberg, J. L.; Hada, M.;

Ehara, M.; Toyota, K.; Fukuda, R.; Hasegawa, J.; Ishida, M.; Nakajima, T.; Honda, Y.; Kitao, O.; Nakai, H.; Vreven, T.; Montgomery, J. A.; Peralta, Jr., J. E.; Ogliaro, F.; Bearpark, M.; Heyd, J. J.; Brothers, E.; Kudin, K. N.; Staroverov, V. N.; Keith, T.; Kobayashi, R.; Normand, J.; Raghavachari, K.; Rendell, A.; Burant, J. C.; Iyengar, S. S.; Tomasi, J.; Cossi, M.; Rega, N.; Millam, J. M.; Klene, M.; Knox, J. E.; Cross, J. B.; Bakken, V.; Adamo, C.; Jaramillo, J.; Gomperts, R.; Stratmann, R. E.; Yazyev, O.; Austin, A. J.; Cammi, R.; Pomelli, C.; Ochterski, J. W.; Martin, R. L.; Morokuma, K.; Zakrzewski, V. G.; Voth, G. A.; Salvador, P.; Dannenberg, J. J.; Dapprich, S.; Daniels, A. D.; Farkas, O.; Foresman, J. B.; Ortiz, J. V.; Cioslowski, J.; Fox, D. J.; *Gaussian, Inc.*, Wallingford CT, **2013**.

(54) Silva, A. P.; Moody, T. S.; Wright, G. D. Fluorescent PET (Photoinduced Electron Transfer) Sensors As Potent Analytical Tools. *Analyst*, **2009**, *134*, 2385–2393.

(55) Kabra, P. M.; Lee, H. K. Solid-Phase Extraction And Determination Of Dansyl Derivatives Of Unconjugated And Acetylated Polyamines By Reversed-Phase Liquid Chromatography: Improved Separation Systems For Polyamines In Cerebrospinal Fluid, Urine And Tissue. *Journal of Chromatography,* **1986***, 380,* 19-32.

(56) M. Kamato, N. Umezawa, N. Kato, T. Higuchi, Novel Probes Showing Specific Fluorescence Enhancement on Binding to a Hexahistidine Tag *Chem. Eur. J*. **2008**, *14*, 8004-8012.

(57) Nair, R. R.; Raju, M.; Patel, N. P.; Raval, I. H.; Suresh, E.; Haldar, S.; Chatterjee, P. B. Naked Eye Instant Reversible Sensing of $Cu^{2+}$ and Its in Situ Imaging in Live Brine Shrimp Artemia. *Analyst* **2015**, *140*, 5464-5468.

(58) Raju, M.; Nair, R. R.; Raval, I. H.; Haldar, S.; Chatterjee, P. B. Reporting a New Siderophore Based $Ca^{2+}$ Selective Chemosensor That Works as a Staining Agent in the Live Organism Artemia. *Analyst* **2015**, *140*, 7799-7809.

(59) Yang, Y. X.; Mu, C. L.; Zhang, J. F.; Zhu, W. Y. Determination Of Biogenic Amines In Digesta By High Performance Liquid Chromatography With Precolumn Dansylation. *Analytical Letters*, **2014**, *47*, 1290–1298.

## Figure Legends

**Figure 1**. Mechanochemical synthesis of the boronic acid integrated coumarin dye CB. Molecular structures of cationic spermine and spermidine at neutral pH.

**Figure 2.** (a) Stack of the PXRD profiles of CB and freeze-dried pure AG and hybrid CB@AG hydrogels. Cross-sectional FESEM images of the hydrogels pure AG (b) and hybrid CB@AG (c).

**Figure 3.** SEM-EDX elemental map of CB@AG showing homogeneous distribution of (a) boron and (b) nitrogen in the hybrid matrix. (c) EDX spectrum of CB@AG.

**Figure 4**. Viscoelastic sweep of pure AG and hybrid CB@AG hydrogels at 25 ˚C at constant 1 Hz frequency.

**Figure 5.** Emission spectra of CB@AG at room temperature in presence of (a) different carbohydrates and nucleobases; (b) various cations; (c) different common anions; and (d) various biogenic amines in aqueous medium at physiological pH (20 mM HEPES buffer) upon excitation at 370 nm.

**Figure 6.** (a) Photographs of CB@AG with and without spermine and spermidine at varying pHs. (b) Plots of fluorescence emission maxima of CB@AG against time in presence of spermine/spermidine. (c) Bar diagrams showing fluorescence maxima of CB@AG and spermine in presence of other biogenic amines in aqueous medium at pH 7.4 (20 mM HEPES). Each coloumn represents the average of three experiments and error bars are the relative standard deviations.

**Figure 7.** (a) Fluorescence change of CB@AG with increasing concentration of spermine. (b) LOD determination plot of CB@AG in presence of spermine. (c) Photographs showing naked eye observable LOD of CB@AG while detecting spermine and spermidine in aqueous solution.

**Figure 8.** Non-linear curve fitting of the titration data points of CB (20 μM made in 0.25 % DMSO in aqueous HEPES) with varying concentrations of spermine (a) and spermidine (b). Error bars indicate standard deviations of three data sets.

**Figure 9.** Proposed mode of hydrogen binding of spermine (top) and spermidine (bottom) with CB based on single point calculations that have been performed using B3lyp/6-31g(d) level of theory.

**Figure 10.** Time resolved fluorescence decay of aqueous CB (10 μM) in absence and presence spermine. LED excitation at 375 nm was used.

**Figure 11.** Measurements of spermine in urinary samples, blood plasma, and aqueous solutions using the hydrogel CB@AG.

**Figure 12.** Measurements of unknown concentration of aqueous spermine solution utilizing the calibration curves developed using (a) UV detector based HPLC technique; (b) fluorescence detector based HPLC technique; and (c) fluorimetric estimation by CB@AG.

**Scheme 1**. Schematic illustration showing the gelling process of CB incorporated agarose: random AG coils in solution at room temperature; CB incorporated random AG coils at high temperature; ordered CB@AG bundles at low temperature. UV-vis and EDX based characterization showing incorporation of CB inside the matrix. PXRD shows lost in the crystalline nature of CB in the swollen hydrogel. Large interior, found in the SEM image of CB@AG, can easily accommodate CB. Variation of storage modulus (G') and loss modulus (G") of the hydrogels at 25 ˚C against strain and time supports soft nature of the gel after CB incorporation.

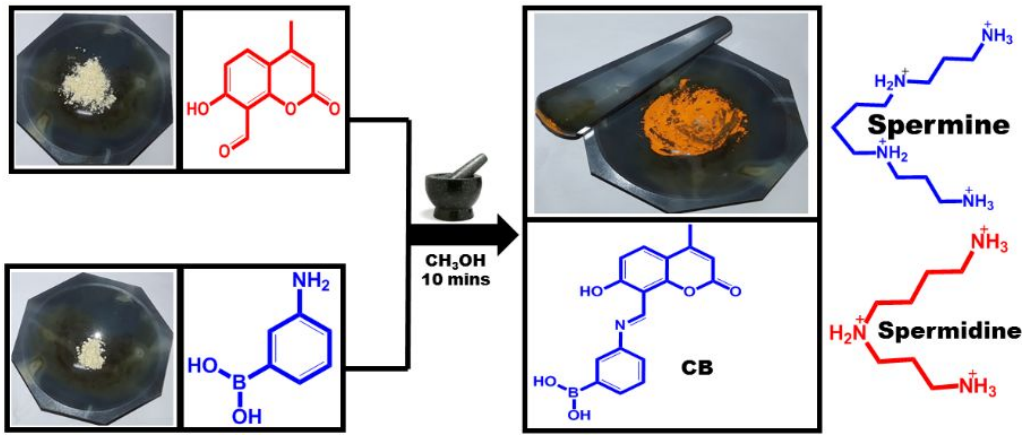
HO
O
O
O
NH2
HO
B
OH
CH3OH
10 mins
HO
O
O
N
HO
B
OH
CB
NH3
H2N
Spermine
NH2
NH3
NH3
H2N
Spermidine
NH3

**Figure 1**

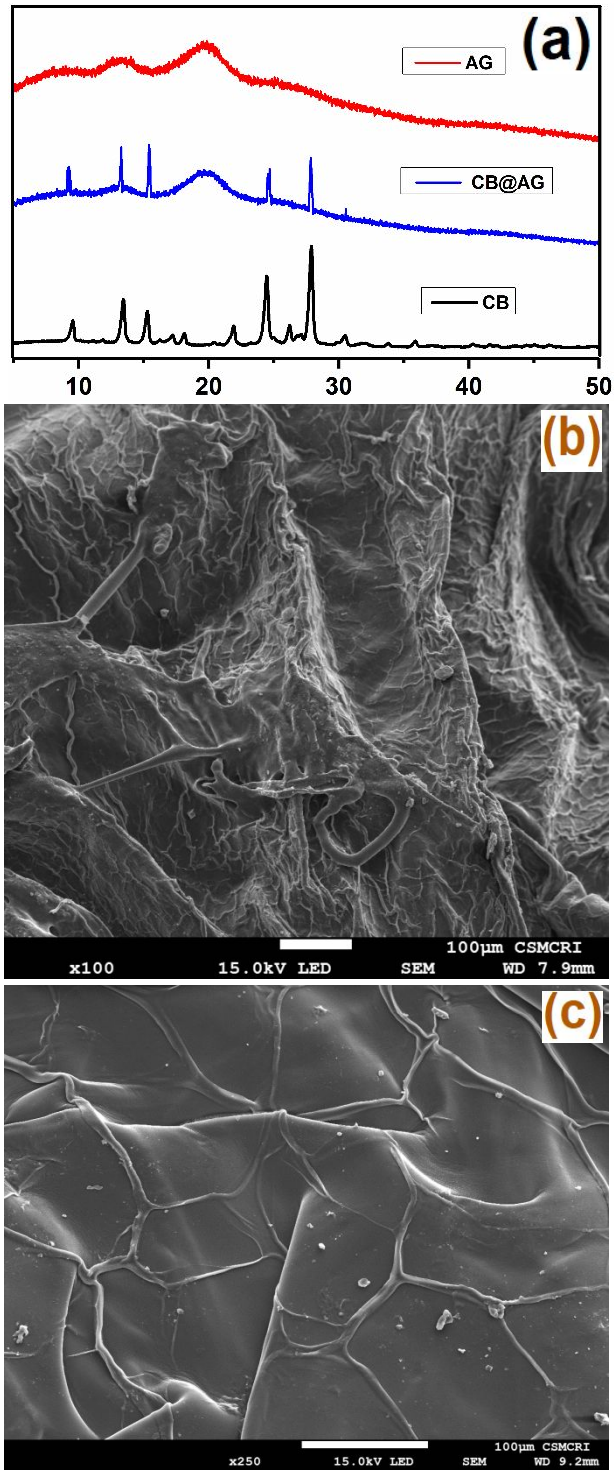
(a)
AG
CB@AG
CB
10
20
30
40
50
(b)
100µm CSMCRI
x100
15.0kV LED
SEM
WD 7.9mm
(c)
100µm CSMCRI
x250
15.0kV LED
SEM
WD 9.2mm

**Figure 2**

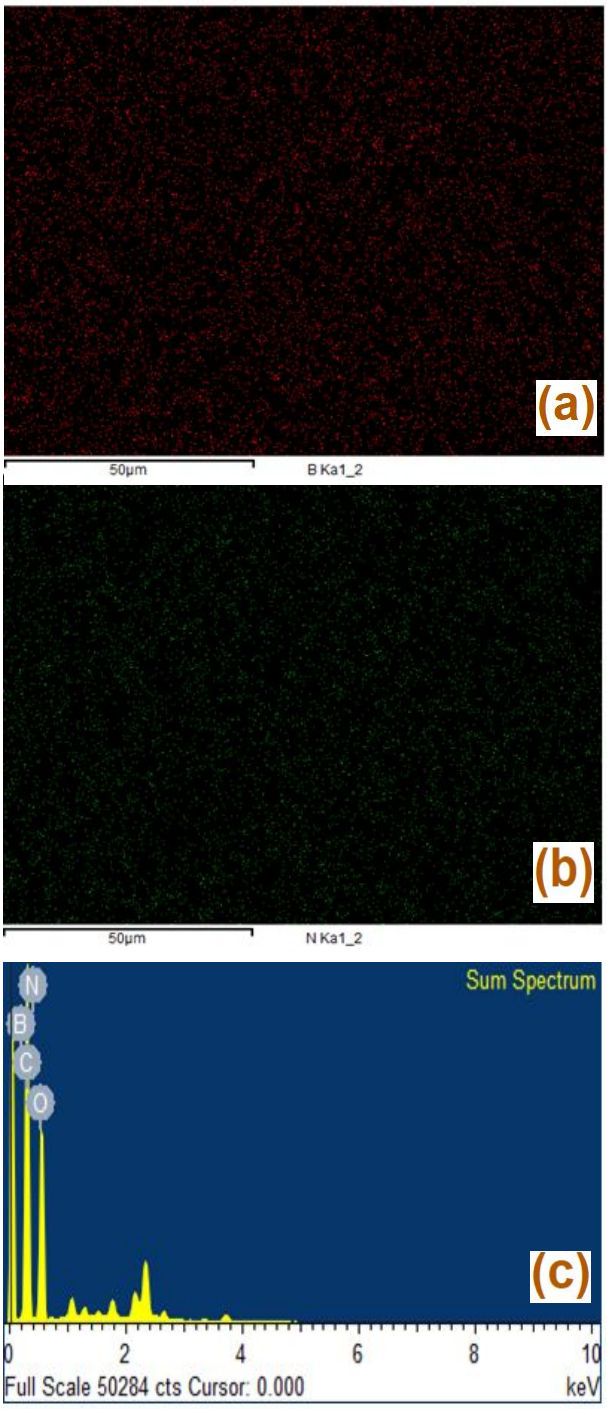
(a)
50µm
B Ka1_2
(b)
50µm
N Ka1_2
Sum Spectrum
N
B
C
O
(c)
0
2
4
6
8
10
Full Scale 50284 cts Cursor: 0.000
keV

**Figure 3**

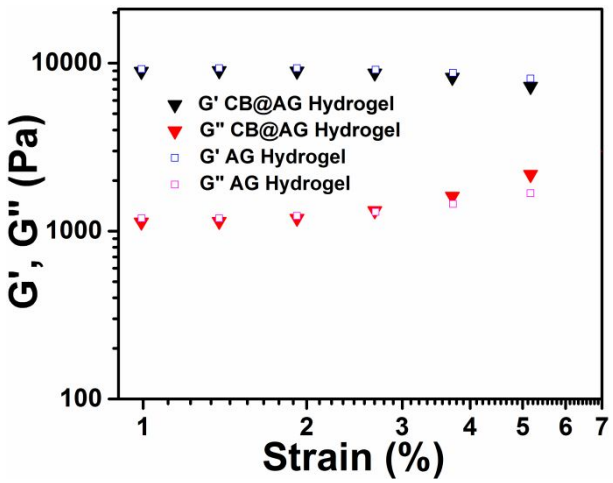
10000
1000
100
G', G'' (Pa)
1
2
3
4
5
6
7
Strain (%)
G' CB@AG Hydrogel
G'' CB@AG Hydrogel
G' AG Hydrogel
G'' AG Hydrogel

**Figure 4**

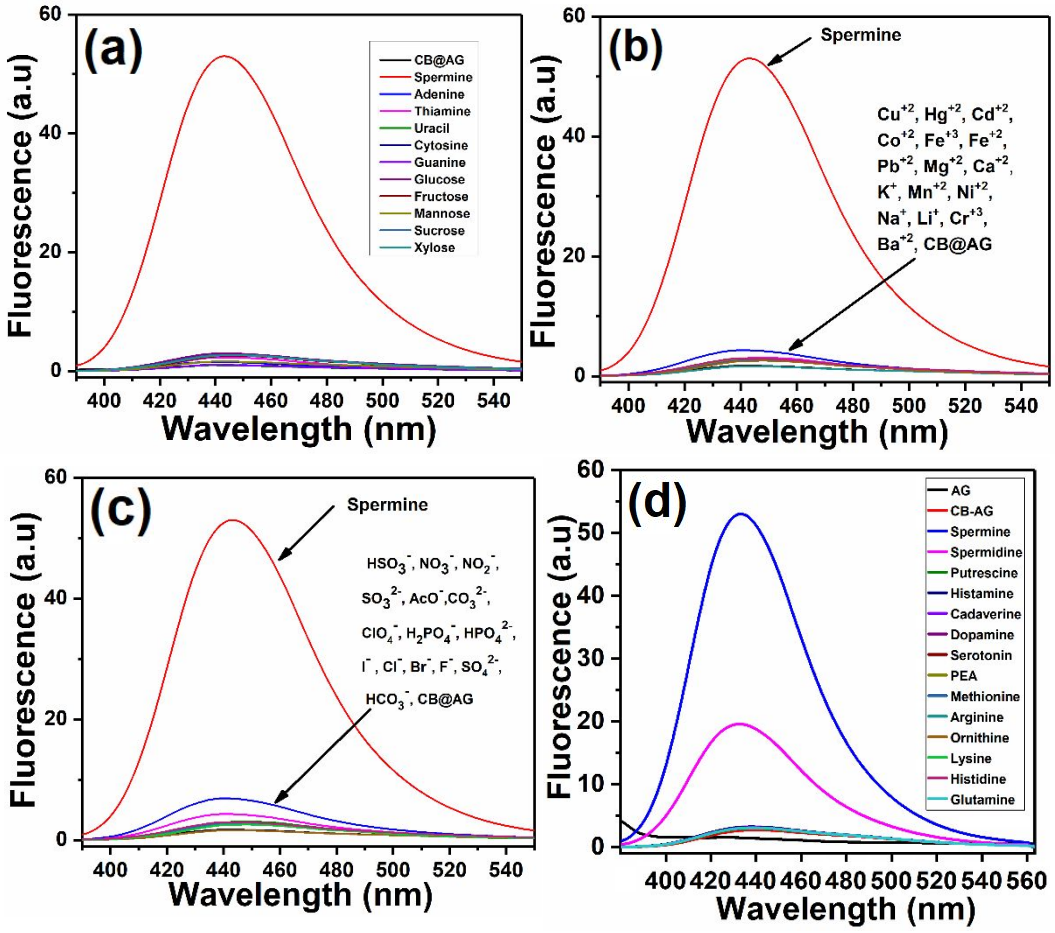
(a)
CB@AG
Spermine
Adenine
Thiamine
Uracil
Cytosine
Guanine
Glucose
Fructose
Mannose
Sucrose
Xylose
Fluorescence (a.u)
Wavelength (nm)
(b)
Spermine
Cu+2, Hg+2, Cd+2,
Co+2, Fe+3, Fe+2,
Pb+2, Mg+2, Ca+2,
K+, Mn+2, Ni+2,
Na+, Li+, Cr+3,
Ba+2, CB@AG
(c)
Spermine
HSO3-, NO3-, NO2-,
SO32-, AcO-,CO32-,
ClO4-, H2PO4-, HPO42-,
I-, Cl-, Br-, F-, SO42-,
HCO3-, CB@AG
(d)
AG
CB-AG
Spermine
Spermidine
Putrescine
Histamine
Cadaverine
Dopamine
Serotonin
PEA
Methionine
Arginine
Ornithine
Lysine
Histidine
Glutamine

**Figure 5**

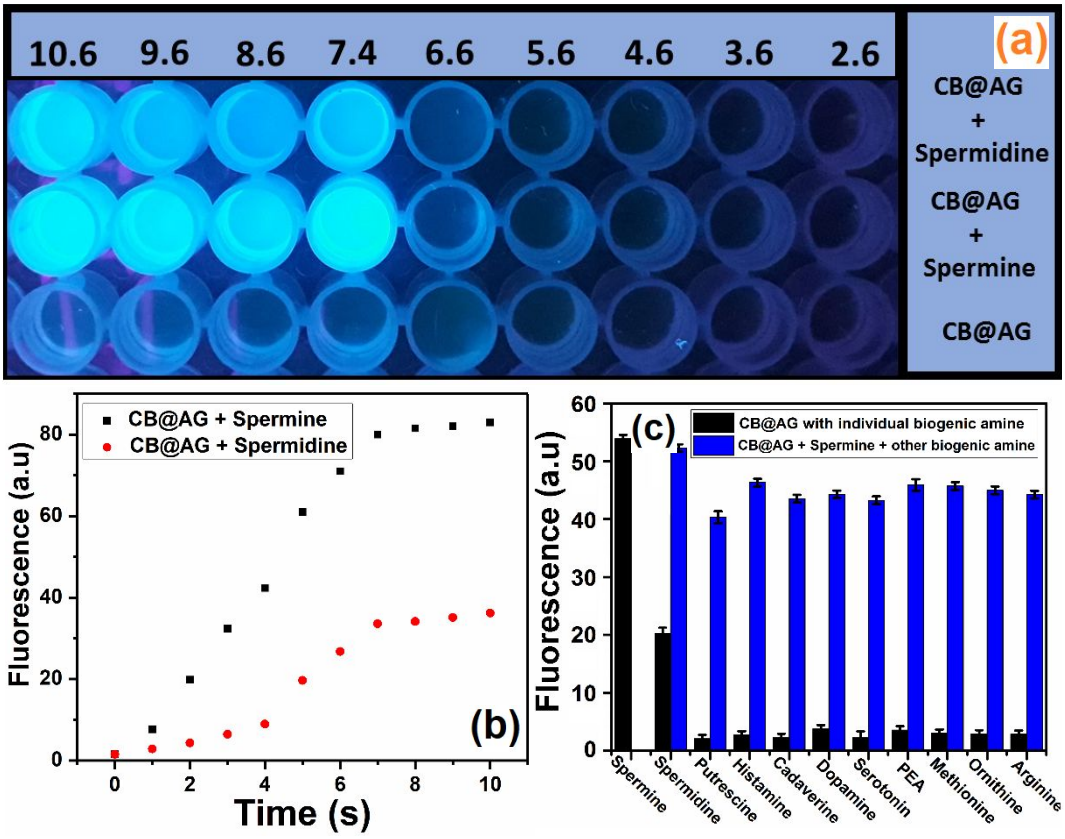
10.6
9.6
8.6
7.4
6.6
5.6
4.6
3.6
2.6
(a)
CB@AG + Spermidine
CB@AG + Spermine
CB@AG
CB@AG + Spermine
CB@AG + Spermidine
Fluorescence (a.u)
Time (s)
(b)
(c)
CB@AG with individual biogenic amine
CB@AG + Spermine + other biogenic amine
Fluorescence (a.u)
Spermine
Spermidine
Putrescine
Histamine
Cadaverine
Dopamine
Serotonin
PEA
Methionine
Ornithine
Arginine

**Figure 6**

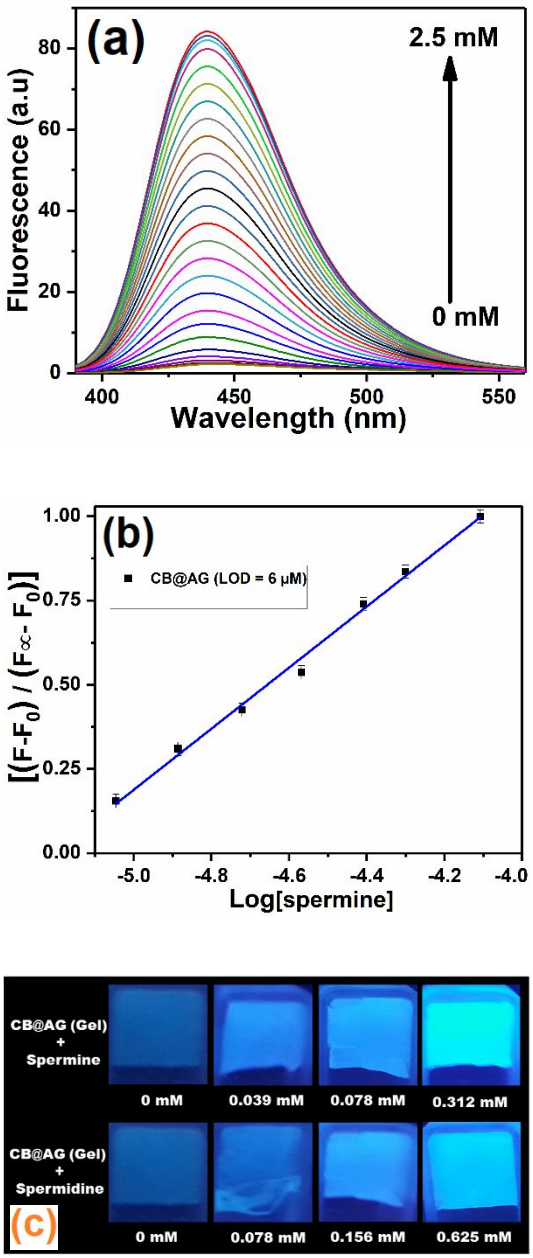
(a)
2.5 mM
0 mM
Fluorescence (a.u)
Wavelength (nm)
(b)
CB@AG (LOD = 6 μM)
[(F-F0) / (F∞- F0)]
Log[spermine]
CB@AG (Gel) + Spermine
0 mM
0.039 mM
0.078 mM
0.312 mM
CB@AG (Gel) + Spermidine
0 mM
0.078 mM
0.156 mM
0.625 mM
(c)

**Figure 7**

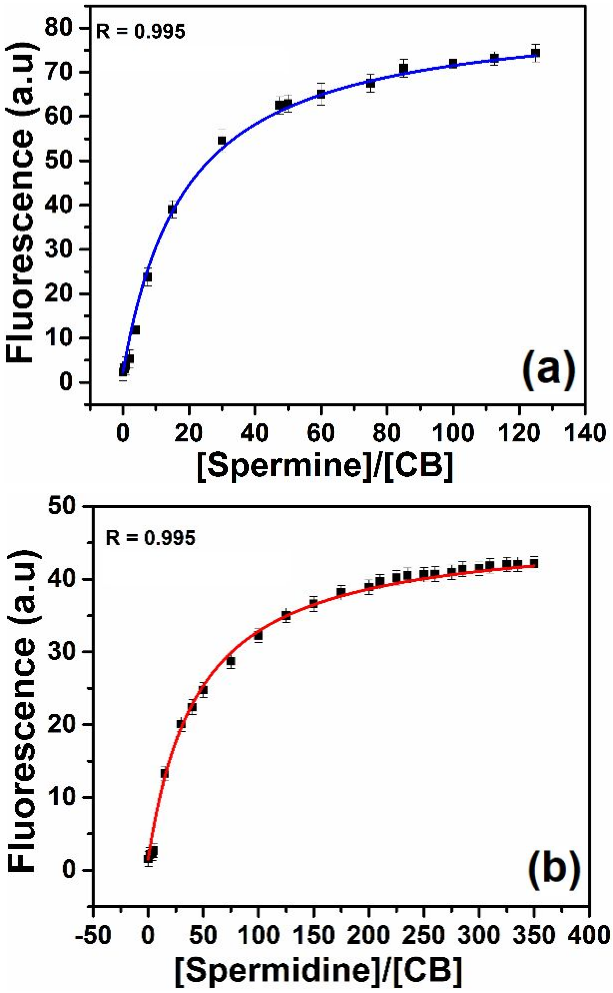
R = 0.995
Fluorescence (a.u)
[Spermine]/[CB]
(a)
R = 0.995
Fluorescence (a.u)
[Spermidine]/[CB]
(b)

**Figure 8**

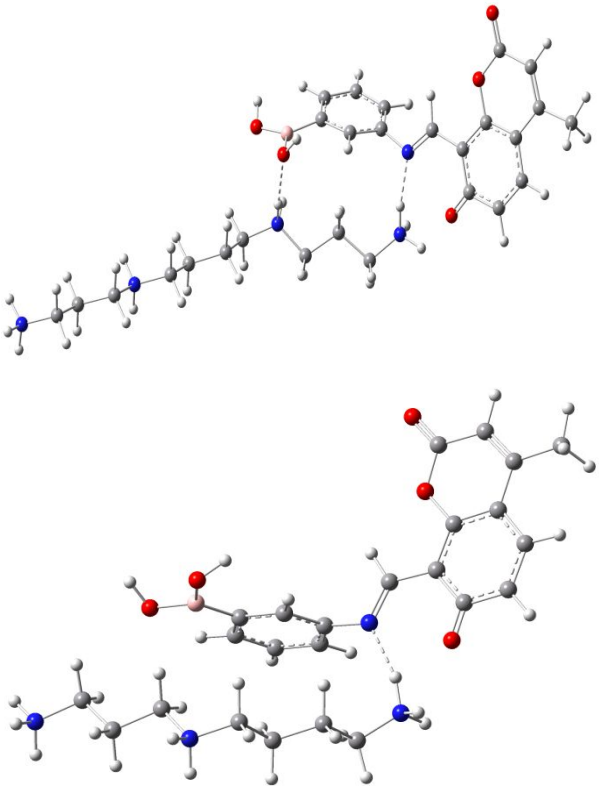

**Figure 9**

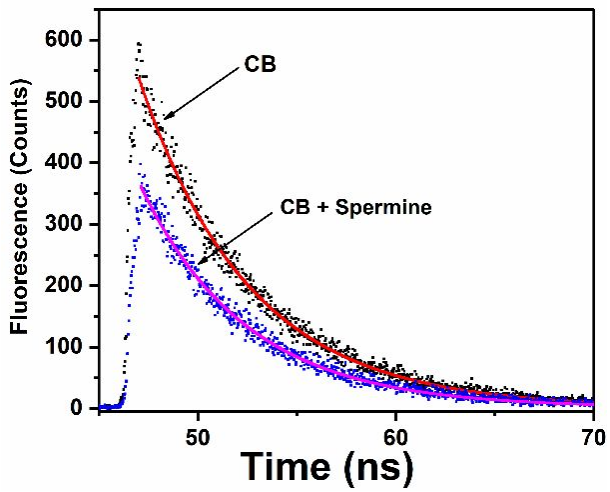
CB
CB + Spermine
Fluorescence (Counts)
Time (ns)
0
100
200
300
400
500
600
50
60
70

**Figure 10**

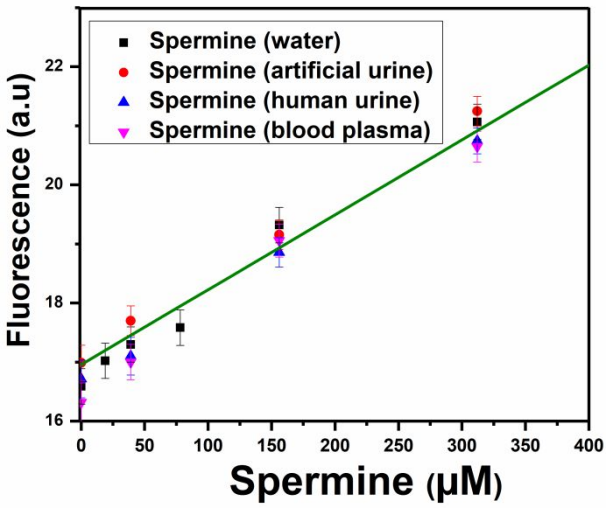
Spermine (water)
Spermine (artificial urine)
Spermine (human urine)
Spermine (blood plasma)
Fluorescence (a.u)
Spermine (μM)
16
18
20
22
0
50
100
150
200
250
300
350
400

**Figure 11**

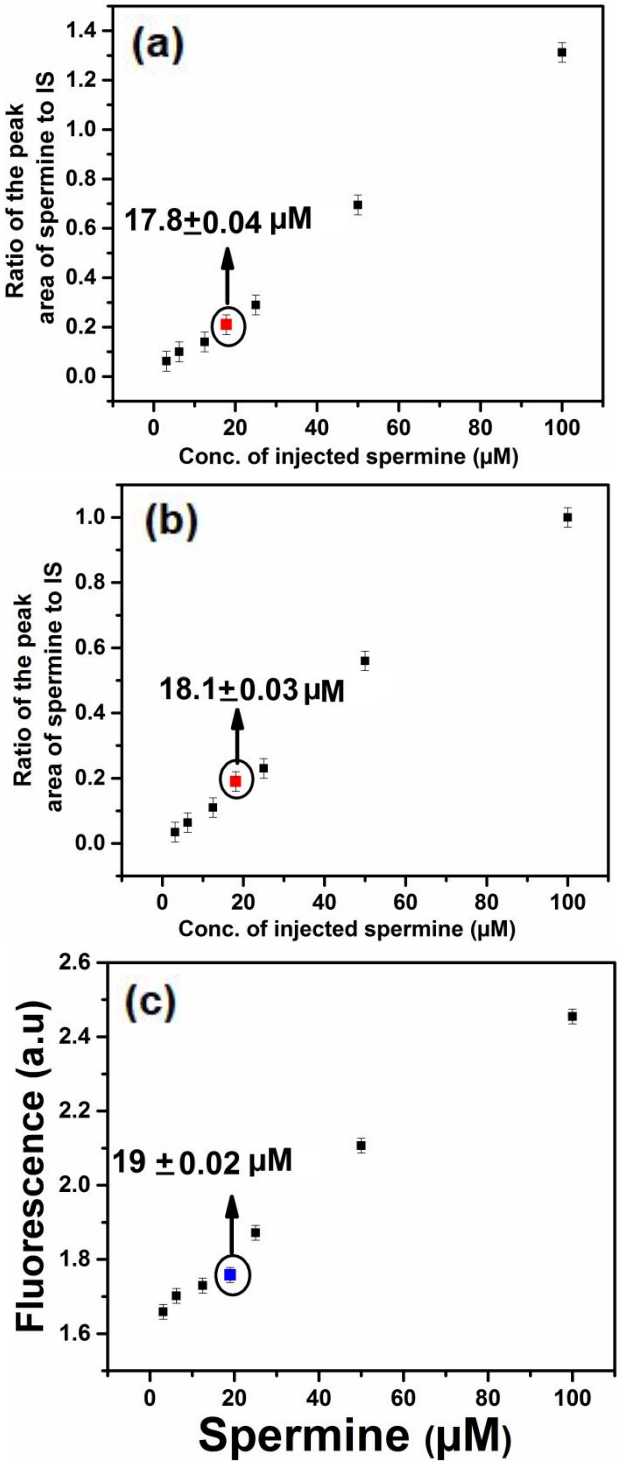
(a)
Ratio of the peak area of spermine to IS
17.8±0.04 µM
Conc. of injected spermine (µM)
(b)
Ratio of the peak area of spermine to IS
18.1±0.03 µM
Conc. of injected spermine (µM)
(c)
Fluorescence (a.u)
19 ±0.02 µM
Spermine (µM)

**Figure 12**

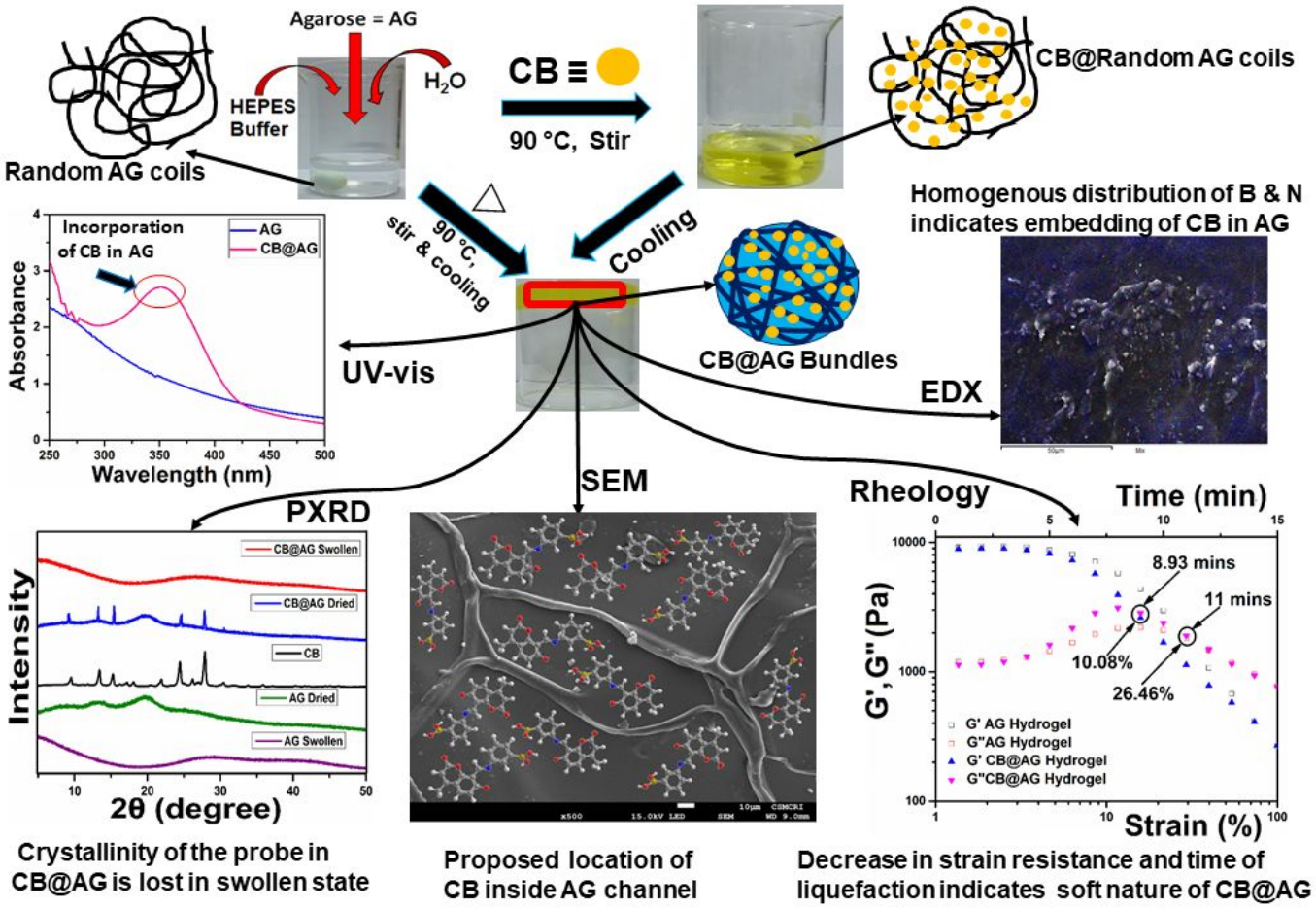
Agarose = AG
HEPES Buffer
$H_2O$
CB ≡
90 °C, Stir
Random AG coils
CB@Random AG coils
90 °C, stir & cooling
Cooling
Homogenous distribution of B & N indicates embedding of CB in AG
Incorporation of CB in AG
AG
CB@AG
Absorbance
Wavelength (nm)
UV-vis
CB@AG Bundles
EDX
SEM
PXRD
Rheology
Time (min)
CB@AG Swollen
CB@AG Dried
CB
AG Dried
AG Swollen
Intensity
2θ (degree)
8.93 mins
11 mins
10.08%
26.46%
G' AG Hydrogel
G"AG Hydrogel
G' CB@AG Hydrogel
G"CB@AG Hydrogel
G', G" (Pa)
Strain (%)
Crystallinity of the probe in CB@AG is lost in swollen state
Proposed location of CB inside AG channel
Decrease in strain resistance and time of liquefaction indicates soft nature of CB@AG

**Scheme 1**

Table 1. Comparison of sensing properties of CB@AG with different spermine/spermidine selective optical probes.

| Probe | Nature of the materials | Detection technique | Limit of detection | Interference from other species | Working range | Application | Reference |
|---|---|---|---|---|---|---|---|
| Agarose-coumarin hydrogel (CB-AG) | 7.4/water | Fluorescence turn on | 6 μM | No Interference | 6 μM-2.5 mM | Human plasma and urine | This study |
| Montmorillonite-coumarin/guanidine hydrogel | 7.4/water | Fluorescence quenching | 20 μM | Cadaverine, putrescine, etc. | 20-100 μM | Artificial urine | 14 |
| Anthryl doped PPE (polyanionic poly(p-phenylene ethynylene) polymer | 5.5/ethanol-water (1:1) | Absorbance & Fluorescence turn on | N.A | Other multicationic polyamines | 0-83 μM | N.A | 15 |
| Tyrosine functionalized gold nanoparticles | 6/water | Absorbance & Fluorescence turn on | 136 & 636 pM | No Interference | 0.1-100 μM & 10-130 nM | Human plasma and urine | 16 |
| Polymer/chitosan/oleic acid based micelles | 7.4/water | Turn On | 10 μM | All polyamines | 10–50 μM | Milk & Yogurt | 17 |
| PFBT-MI polymer-surfactant SDS self-assembled system | Water/ surfactant | Turn Off | 0.33 μM | Putrescine, dimethylethylenediamine | 0.33-120 μM | Human urine | 18 |
| Gold nanoparticles based | Water | Abs | 10 ppb | N.A | N.A | Human urine | 19 |
| Pyrene derivative & squarine containing self-assenbled system | 7.4/water | Fluorescence Quenching (0-20 μM) | 20 μM | No Interference | 20-100 μM | Human urine | 20 |

| | | | | | | | |
|---|---|---|---|---|---|---|---|
| Pillar[5]arene functionalized silver nanoparticles | Water | UV-vis | 200 nM | Different polyamines | N.A | N.A | 21 |
| Functionalized HPTS based self-assembled system | 7.2/water | Turn off | N.A | No Interference | N.A | Artificial urine | 22 |
| BODIPY functionalized gold nanoparticles | Water | Turn on | N.A | N.A | 0-100 μM | Artificial urine | 23 |
| Copper complex of organic nanoparticles | DMF/$H_2O$ | Abs | 35 & 36.2 nM | No Interference | 0-2.6 μM | Mushroom and meat | 24 |
| Cucurbituril-perylenediimide based supramolecular amphiphile | | Turn off | 5 μM | Putrescine | 5–60 μM | | 25 |
| Thiophene copolymer coated CdTe QDs and heparin conjugate | 7.4/water | Turn on | 2.90 & 1.66 nM | Data with different biogenic amines is not available | 0–15 μM | Human serum | 26 |
| AIEgen@ cucurbit[7]uril based supramolecular system | DMSO-water mixture | Turn off | 1 μM | Adaman tanamine | 1-40 μM | | 27 |
| Ag-Au/AgCl nanohybrid | 7.4/water | Turn off | 0.87 nM | NaCl, BSA, GSH | N.A | | 28 |
| DAB-PDI perylenediamine based self-assembled system | $CH_3CN$/ $H_2O$/SDS | Absorbance & Fluorescence turn on | 27.5 nM | No Interference | 27.5 nM - 120 μM | N.A | 29 |

| | | | | | | | |
|---|---|---|---|---|---|---|---|
| DNA aptamer coated gold nanoparticles | 3.29/water | Abs | 15.25 nM | Histamine | 0-5 µM | Artificial & clinical urine | 30 |
| ctDNA gold nanoparticles | 9.91/water | Abs | 11.6 nM | Cadaverine, spermidine, histamine | 11.6 nM - 2.0 µM | Beef and chrysanthemum | 31 |
| ssDNA-capped gold nanoparticles | 3.29/water | Abs | 13.9 nM | No Interference | N.A | Human plasma and urine | 32 |
| Complexes of Pb(II), Cd(II), & Zn(II) | 7.6/water | Turn on | 25 µM | Different Polyamines | 25-2500 µM | | 33 |
| Crown ether based organic compounds | $CH_3OH$ | Abs | N.A | N.A | N.A | | 34 |

Table 2. Quantum yield ($\Phi_f$), lifetime ($\tau$), and radiative and total non-radiative rate constant ($k_r$ and $k_{nr}$) values, where $\chi^2$ represents the fitting parameter.

| **Sample** | **τ (ns)** | **$\chi^2$** | **$\Phi_f$** | **$k_r$ ($10^8$ $s^{-1}$)** | **$k_{nr}$ ($10^8$ $s^{-1}$)** |
|---|---|---|---|---|---|
| CB | 5.51 | 1.02 | 0.012 | 0.02 | 1.79 |
| CB with spermine | 5.35 | 1.02 | 0.218 | 0.41 | 1.46 |

## TOC Graphic

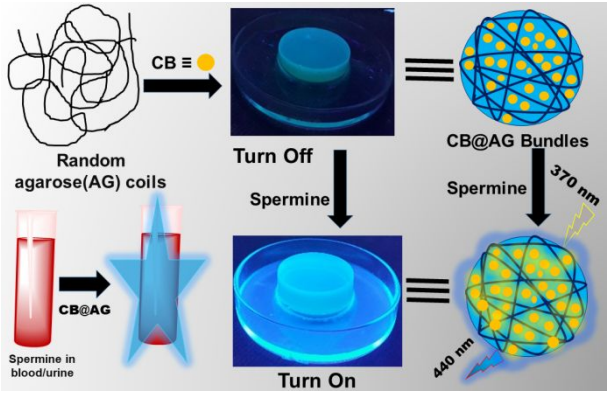
CB ≡
Random
agarose(AG) coils
Turn Off
CB@AG Bundles
Spermine
Spermine
370 nm
CB@AG
Spermine in
blood/urine
Turn On
440 nm